

Anti-Stokes photoluminescence and optical cooling of CdSeS/ZnS colloidal quantum dots embedded in dielectric waveguides

Mark V. Reymatias¹, Gema J. Alas¹, Arjun Senthil¹, Sami A. Nazib¹,
Troy A. Hutchins-Delgado¹, Hosuk Lee¹, Shruti I. Gharde¹, Dominic Bosomtwi¹,
DeYannah J. Walker¹, Adreanna Rael¹, Nathan J. Withers¹, Gennady A. Smolyakov¹,
Alexander Neumann², Yuliya Kuznetsova², Sergei A. Ivanov³, Dale L. Huber⁴, and Marek Osiński¹

¹Center for High Technology Materials, University of New Mexico, 1313 Goddard SE,
Albuquerque, New Mexico 87106-4343, USA

²Picotek LLC, 3059 Dona Juanita Drive SW, Albuquerque, NM 87121, USA

³Center for Integrated Nanotechnologies, Los Alamos National Laboratory, 1000 Eubank SE,
Albuquerque, New Mexico 87123, USA

⁴Center for Integrated Nanotechnologies, Sandia National Laboratories, 1000 Eubank SE,
Albuquerque, New Mexico 87123, USA

ABSTRACT

Anti-Stokes photoluminescence from colloidal CdSeS/ZnS quantum dots (QDs) is observed. The QDs were inserted into the core of wider-bandgap SiO₂/Si₃N₄/SiO₂ structure by thin film deposition and confirmed as promising nanoemitters for laser cooling due to efficient anti-Stokes emission. The nanoemitters were optically pumped by semiconductor lasers coupled to the waveguides using free-space optics. A direct evidence of local optical cooling in the waveguide structure has been demonstrated with a luminescence thermometry based on the detection of photoluminescence signal phase change versus power of the pumping laser, using a lock-in amplifier.

Keywords: Anti-Stokes photoluminescence; colloidal quantum dots; optical cooling; CdSeS/ZnS quantum dots.

1. INTRODUCTION

Ordinarily, the process of optical excitation and emission in solids results in heat generation in the medium. This is a fundamental effect caused by the Stokes energy shift between the higher-energy pump photons and the lower-energy output photons, often called the quantum defect. In optical refrigeration or laser cooling, radiation cooling is achieved by anti-Stokes fluorescence within the medium that overcomes the heat generated by the Stokes-shifted fluorescence. A laser cooling cycle in a solid is illustrated in Fig. 1. The upper and lower electronic levels (manifolds) are split into many

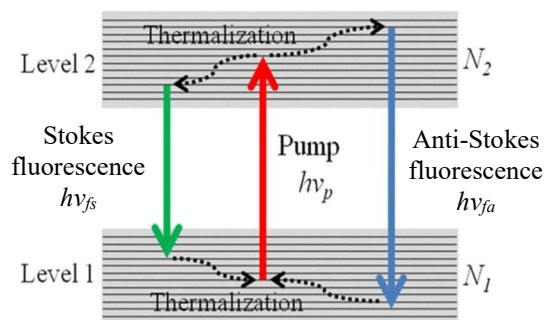


Fig. 1. Energy-level scheme for laser cooling.

closely spaced sublevels (energy bands in case of semiconductor materials). Pump photons at the longer-wavelength side of the absorption spectrum with the energy $h\nu_p$ excite the lower-energy electronic transitions from the ground state to the excited state. The excited ions in a host matrix (or charge carriers in a semiconductor material) exchange energy with phonons during the thermalization process and reach quasi-equilibrium with the lattice. Fluorescence then follows with a mean photon energy $h\nu_{fa}$ higher than that of the originally absorbed photon, thus removing energy from the sample. Several models have been proposed in regards to the thermodynamics of laser cooling [1]-[3].

An essential condition for achieving laser cooling in solids is a low nonradiative recombination rate and availability of a high-quantum-efficiency anti-Stokes transition. It is equally important that the anti-Stokes spontaneous emission escapes the material without trapping and reabsorption, which would cause re-heating of the sample. These requirements can be satisfied for rare-earth ions in hosts with low phonon

energy and low refractive index of the host material, such as fluoride or chloride glasses and crystals [2]. The first experimentally observed instance of laser cooling was reported for Yb³⁺-doped ZBLANP (ZrF₄-BaF₂-LaF₃-AlF₃-NaF-PbF₂) glass [4]. Poor heat conduction of glasses, however, makes them unsuitable for heat sink applications. Thermal conductivity of undoped silica glass is ~1.38 W/(m·K), and even smaller number of ~0.628 W/(m·K) was reported for ZBLAN (ZrF₄-BaF₂-LaF₃-AlF₃-NaF), considered to be the most stable heavy metal fluoride glass and the excellent host for rare-earth ions [5]. In contrast to glasses, III-V compound semiconductors are characterized by much higher thermal conductivity: ~45 W/(m·K) for GaAs; ~68 W/(m·K) for InP; ~36 W/(m·K) for GaSb, and exceptionally high ~319 W/(m·K) for AlN [6]. In semiconductors, however, problems with the realization of laser cooling include relatively high nonradiative recombination rates, low extraction efficiency of spontaneous emission due to the total internal reflection, and the reabsorption effect [7].

Laser cooling of semiconductors has been attempted for decades in III-V semiconductor quantum wells without success. Significant breakthroughs have been recently reported by using II-VI, rather than III-V, nanomaterials. In particular, laser cooling by 40 K has been observed in II-VI CdS nanoribbons [8] and by 30 K in CdS nanobelts [7]. Very intense phonon-assisted anti-Stokes photoluminescence and even lasing has recently been reported in ZnTe nanoribbons [9]. CdSe/ZnS core/shell QDs have been reported as promising for laser cooling applications [10]. The net laser cooling in those II-VI materials was attributed to strong coupling between excitons and longitudinal optical phonons (LOPs) that allowed the resonant annihilation of multiple LOPs in the luminescence up-conversion processes, high external quantum efficiency, and negligible background absorption. These II-VI materials are very promising for development of cooling semiconductor devices.

Realization of the cooling semiconductor device concept can be attempted in any semiconductor material system with high efficiency of anti-Stokes photoluminescence. However, this concept implies very serious requirements for the properties/quality of the material (such as high thermal conductivity, high efficiency of anti-Stokes luminescence, high external quantum efficiency, strong coupling between excitons and LOPs, and negligible background absorption) that are not easy to meet in one specific material.

We adopt an alternative concept of a cooling hybrid device, where nanosize emitters grown in any semiconductor material system (including III-V, II-VI, or IV-VI semiconductors) with high efficiency of anti-Stokes photoluminescence are inserted into an optical waveguide layer made of a wider-bandgap high-thermal-conductivity material. The nanoemitters are optically pumped by the external laser emission and provide cooling, similar to the laser cooling scheme of rare-earth-doped glasses optically pumped with external laser light. This work reports an evidence of optical cooling in a symmetric SiO₂/Si₃N₄/SiO₂ optical dielectric waveguide grown on Si with layers of commercially available CdSeS/ZnS quantum dots (QDs) inserted into the middle section of a Si₃N₄ core.

2. CHARACTERIZATION OF CdSeS/ZnS QUANTUM DOTS

2.1 Materials

CdSeS/ZnS QDs (with peak photoluminescence emission wavelengths of 490 nm, 540 nm, 630 nm, and 665 nm) were purchased from Sigma-Aldrich. The QDs were suspended in toluene at a concentration of 1 mg/mL and were diluted to a concentration of 0.1 mg/mL in toluene or in hexanes before their characterization and use in waveguide fabrication.

2.2 Colloidal QD characterization

Dynamic light scattering (DLS) was performed on the colloidal QDs using a Dynapro Titan (model DP-TH-03) with temperature-controlled Micro Sampler (model TP-DC-04) from Wyatt Technology Corporation with DYNAMICS software version 6.12.0.3 at 298 K. QDs were monomodal polydisperse with a peak of hydrodynamic size at 17.3 nm, as determined via DLS analysis (Fig. 2).

Zeta-potential measurements of the colloidal QDs suspended in toluene were performed at 293 K using a Zetasizer Nano-S (model ZEN2600) from Malvern Instruments Limited (now Malvern Panalytical). Zeta potential peak of 47.5 mV for the CdSeS/ZnS QDs in Fig. 3 indicates their good stability in toluene suspension. The QDs can also be suspended in similar non-polar organic solvents, such as chloroform or hexanes.

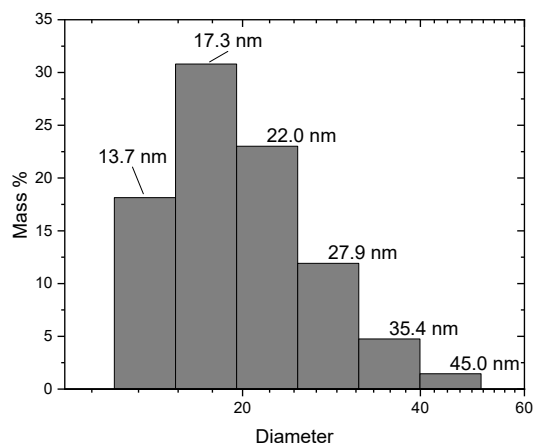


Fig. 2. Dynamic light scattering measurement of CdSeS/ZnS QDs.

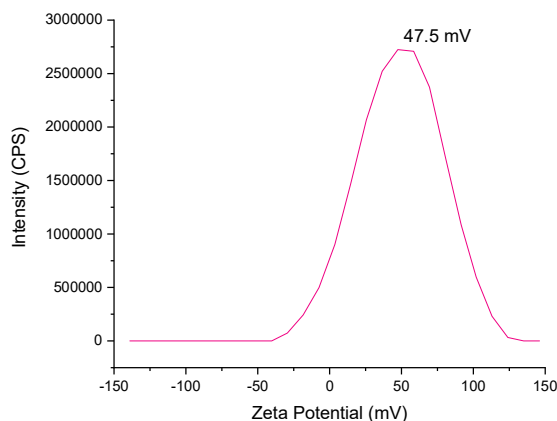


Fig. 3. Zeta potential measurement of CdSeS/ZnS in toluene.

2.3 Anti-Stokes photoluminescence measurements

Anti-Stokes photoluminescence (ASPL) scans were performed on colloidal CdSeS/ZnS QDs using a Horiba-Jobin Yvon Fluorolog spectrofluorometer with Fluorescence 3.9 software. Unless otherwise noted, all PL scans on the QDs were performed with emission and excitation slit widths of 1 nm and were measured with 1-nm wavelength steps at 298 K.

To identify optimal excitation wavelengths of CdSeS/ZnS QDs for anti-Stokes photoluminescence, PL and photoluminescence excitation (PLE) scans were performed for CdSeS/ZnS QDs of all four emission wavelengths. First, PL scans at 350 nm excitation were performed to determine the exact peak of emission of the QDs [Fig. 4(a)]. Subsequently, PLE scans were performed at the identified emission peak wavelengths to readily identify both Stokes and anti-Stokes excitation wavelengths at the observed emission wavelength [Fig. 4(b)].

As determined for the 490-nm emitting CdSeS/ZnS QDs, there were no readily identifiable anti-Stokes excitation peaks for the emission peak of 491 nm – therefore, the excitation wavelength had to be increasingly varied towards the tail-end of the emission peak to observe ASPL. Fig. 5 shows Stokes and anti-Stokes PL scans for 490-nm emitting CdSeS/ZnS QDs with increasing excitation wavelengths – by progressively increasing the excitation wavelength, an optimal anti-Stokes to Stokes photoluminescence signal ratio could be identified. In the case of the 490-nm emitting CdSeS/ZnS QDs, the aforementioned optimal ratio was obtained with 511 nm excitation.

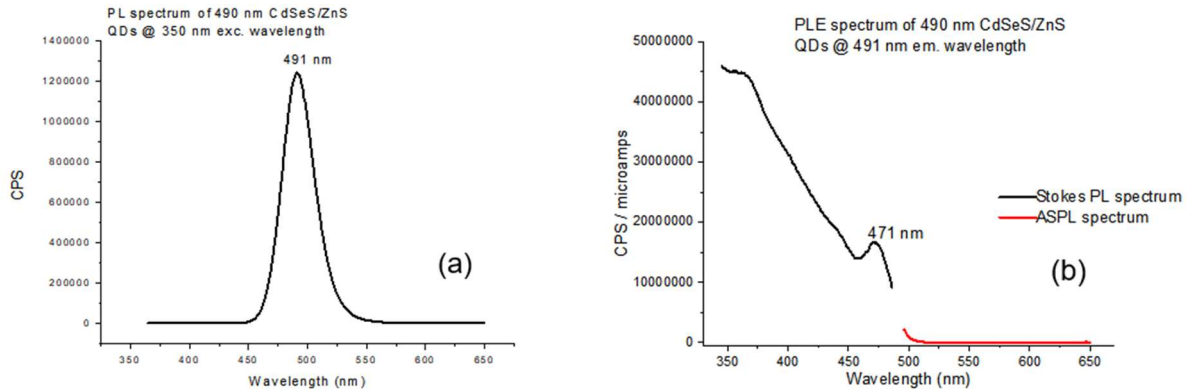


Fig. 4. (a) PL scan of 490-nm emitting CdSeS/ZnS QDs excited by 350 nm wavelength light; and (b) PLE scan of 490-nm emitting CdSeS/ZnS QDs observed at 491 nm wavelength emission.

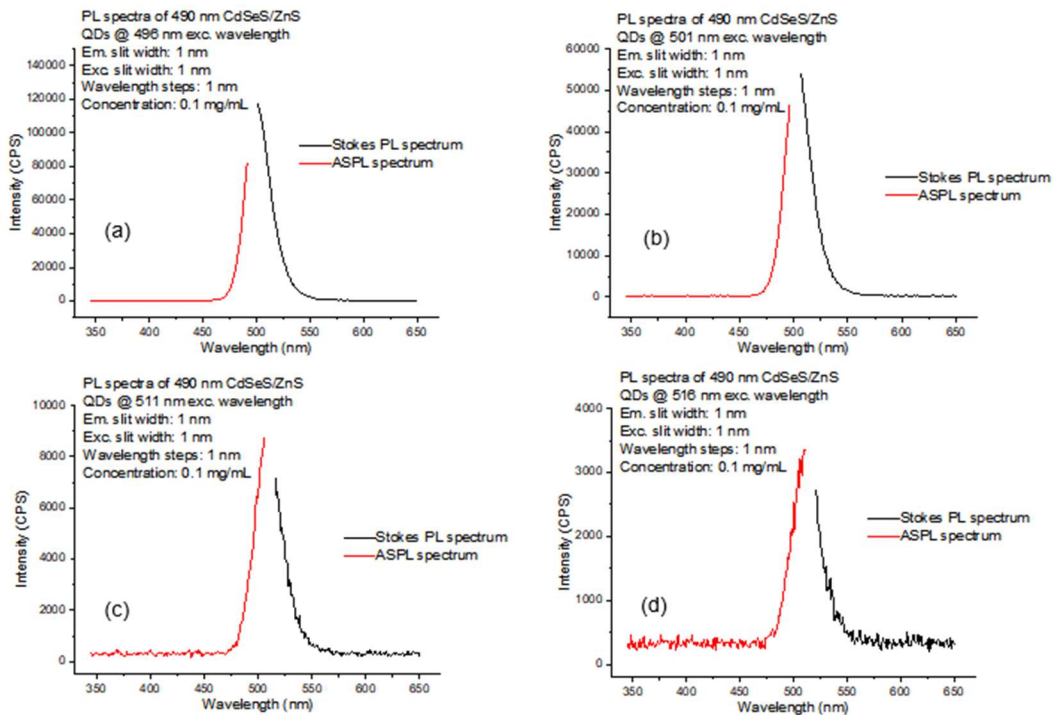


Fig. 5. Stokes and anti-Stokes photoluminescence scans of 490-nm emitting CdSeS/ZnS QDs at the excitation wavelengths of (a) 496 nm, (b) 501 nm, (c) 511 nm, and (d) 516 nm.

The above process, illustrated in Fig. 5, was repeated for QD samples of the three remaining peak-emission wavelengths (540 nm, 630 nm, and 665 nm). While Fig. 6 depicts the 490-nm emitting CdSeS/ZnS QDs to have the highest anti-Stokes to Stokes photoluminescence signal ratio, the 630-nm emitting CdSeS/ZnS QDs were selected to be embedded in the waveguide as the laser cooling apparatus was optimized for red excitation light. The 630-nm emitting CdSeS/ZnS QDs were suspended in hexanes before further characterization and waveguide fabrication.

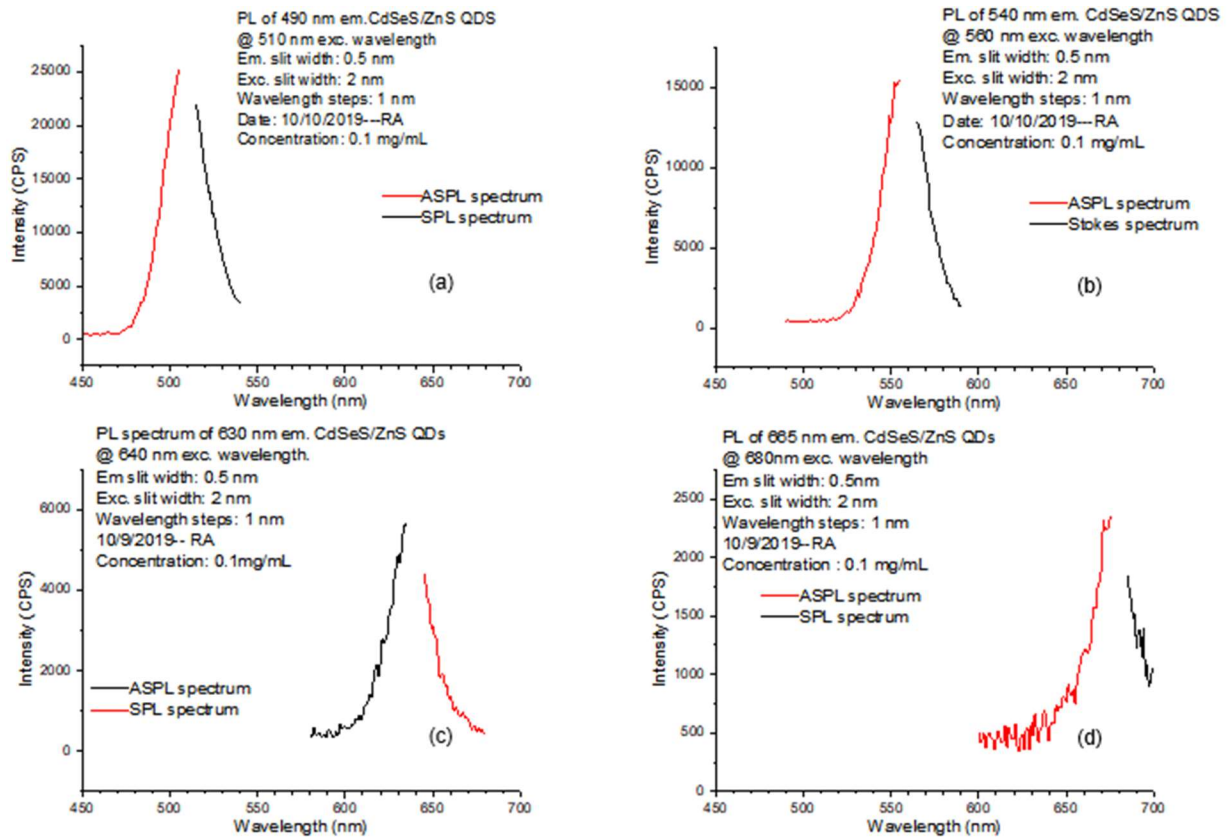


Fig. 6. Stokes and anti-Stokes photoluminescence scans of CdSeS/ZnS QDs emitting at 490 nm, 540 nm, 630 nm, and 665 nm at the excitation wavelengths of (a) 510 nm, (b) 560 nm, (c) 640 nm, and (d) 680 nm, respectively.

2.4 Optical characterizations of selected QDs

2.4.1 Absorption spectrum of CdSeS/ZnS QDs

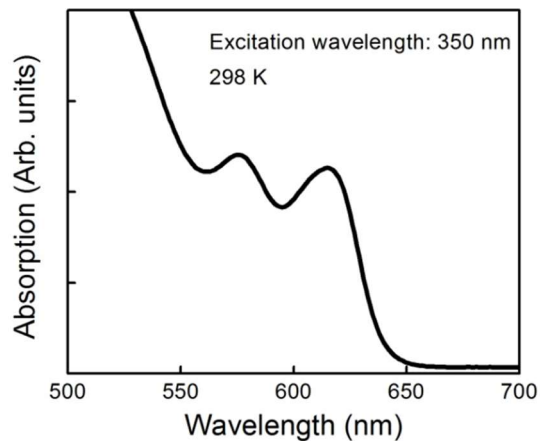


Fig. 7. Absorption spectrum of 630-nm emitting CdSeS/ZnS QDs.

Absorbance of the colloidal QDs was determined using a Varian Cary-5000 spectrophotometer with Varian UV software version 3.00 from Varian, Inc. (now Agilent Technologies) at 298 K. Absorption spectrum of 630-nm emitting CdSeS/ZnS QDs is shown in Fig. 7. The double-peaked absorption at 575 nm and 615 nm near the bandgap edge corresponds to two closely spaced excitation levels in QDs, which is a necessary condition for anti-Stokes refrigeration [11]. These QDs demonstrated relatively strong anti-Stokes PL, as shown below.

2.4.2 Temperature dependent Stokes anti-Stokes photoluminescence of CdSeS/ZnS QDs

Temperature dependent Stokes anti-Stokes photoluminescence scans were performed on colloidal CdSeS/ZnS QDs in hexane using a Horiba-Jobin Yvon Fluorolog spectrofluorometer with Fluorescence 3.9 software. The temperature variation range was set to be from 278 K to 328 K with 10 K steps, considering the boiling point of hexane of 341 K. For this temperature range, when excited at 350-nm wavelength, the PL peak red-shifted from 624.8 nm (1.984 eV) to 628.8 nm (1.971 eV), while its intensity was reduced by 36% and its full width at half maximum (FWHM) was increased from 79.4 meV to 85.6 meV [Fig. 8(a)]. The temperature dependence of these QD was calibrated to be -0.46 meV K^{-1} at 350 nm excitation. The PL peak broadening and intensity decrease with red shift are typical in temperature-dependent PL from semiconductors, when moving from lower to higher temperatures.

As expected, increasing the excitation wavelength to 658 nm to generate anti-Stokes PL [Fig. 8(b)] resulted in a significant decrease in PL intensity as compared to Stokes PL emission intensity. However, the temperature dependence of anti-Stokes PL intensity is opposite to that excited at the wavelength of 350 nm, namely, the peak intensity is enhanced more than twice with temperature increasing from 278 K to 328 K. This could be interpreted as anti-Stokes effects associated with the two photoexcitations observed in the absorption spectrum of Fig. 7 under high population of phonons at elevated temperatures [11]. Fig. 8(b), therefore, provides clear evidence that the 630-nm emitting CdSeS/ZnS QDs demonstrate strong anti-Stokes effects suitable for laser cooling.

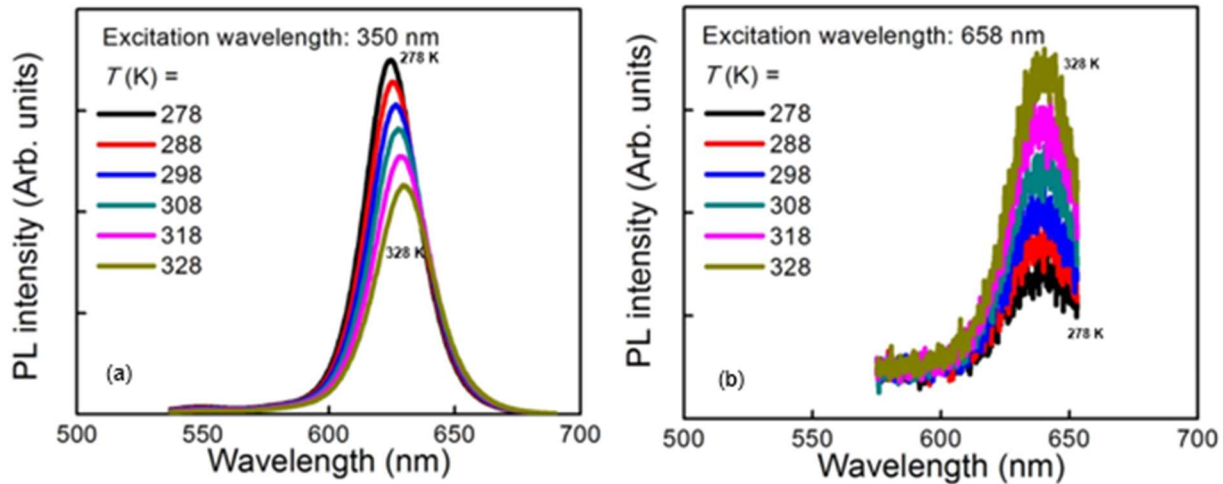


Fig. 8. (a) Stokes PL scans of 630-nm emitting CdSeS/ZnS QDs at excitation wavelength of 350 nm at temperatures ranging from 278 K to 328 K; and (b) ASPL scans of the same QDs at excitation wavelength of 658 nm at temperatures ranging from 278 K to 328 K.

3. QUANTUM-DOT-EMBEDDED WAVEGUIDE FABRICATION AND CHARACTERIZATION

3.1 CdSeS/ZnS-QD-embedded waveguide simulation

Simulations of a $\text{SiO}_2/\text{Si}_3\text{N}_4/\text{SiO}_2$ waveguide with embedded CdSeS/ZnS QDs emitting at 630 nm were performed using Optiwave and RSoft finite element and FDTD software packages. In the simulations, the waveguide was placed on a silicon substrate and surrounded by air and. Table 1 references the layer-by-layer material composition of the waveguide, along with their corresponding thicknesses and refractive indices used in the simulation. For the QD layer, the refractive index was calculated with the assumption that the QDs reach a maximum packing density of 73%, with the remaining 27% composed of SiO_2 to encase the QDs (as described in the next subsection).

Fig. 9 shows the transverse refractive index profile and the fundamental TE-like mode of the waveguide structure. Spatial profile of intensity in the strongest E_x field component is shown and information about the calculated effective modal index is provided. Strong confinement of the fundamental TE-like mode of the waveguide structure is obvious from the figure.

Fig. 10 shows the results of 3D FDTD simulation of the fundamental TE-like mode propagation in the waveguide structure. The mode is represented by the E_x and H_y component distributions at fixed y -positions of interest. The mode was launched in the positive z direction at $z = 0$. As it can be seen from the figure, the mode stays well confined to the waveguide along the propagation direction.

Table 1. Simulation parameters for waveguide materials, listed in order from top (air) to bottom (silicon substrate)

Material	Thickness (nm)	Refractive index at 630 nm
SiO ₂	1000	1.4571
Si ₃ N ₄	1000	2.0398
QDs	25	2.3465
Si ₃ N ₄	1000	2.0398
SiO ₂	3000	1.4571

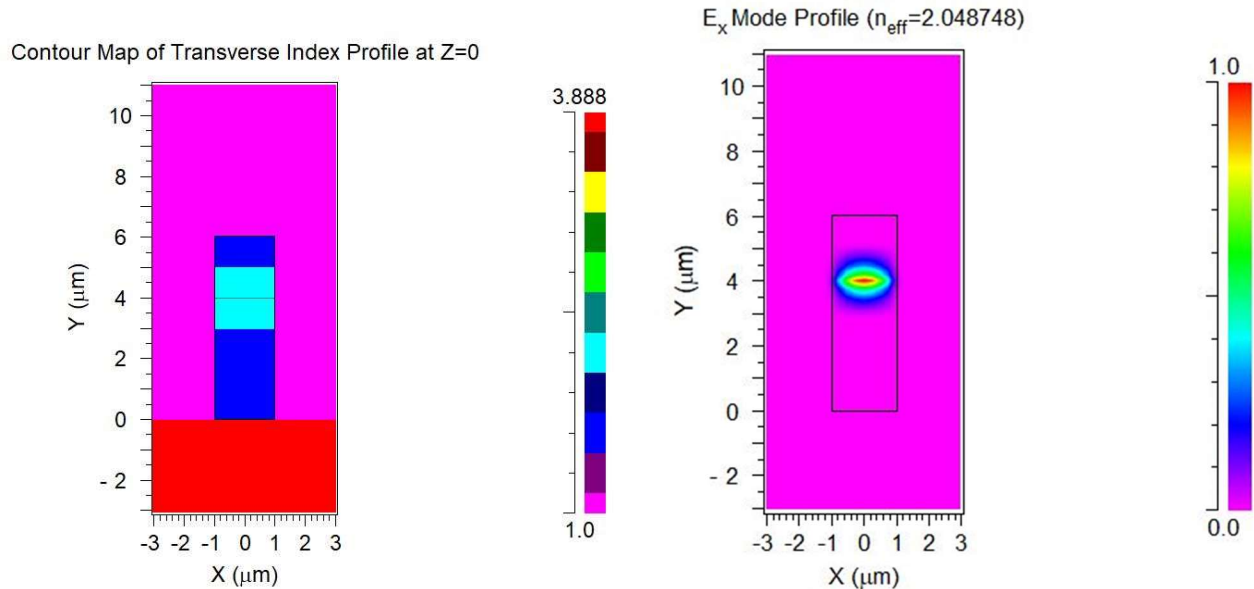


Fig. 9. Transverse refractive index profile (left) and E_x component of the fundamental TE-like mode (right) of the waveguide structure.

3.2 CdSeS/ZnS-QD-embedded waveguide fabrication

Fig. 11 shows scanning electron microscope (a) and optical (b) microscope images of the waveguide (b) and observed PL from the corresponding areas with 450 nm light excitation at room temperature (c) in top-down (upper panels) and cross-sectional views (bottom panels). The layer structure for the designed 8- μm -thick QD-embedded waveguide was 3- μm SiO₂/6- μm Si₃N₄/1- μm SiO₂ on a Si(001) substrate. The QD layer indicated with an arrow was embedded in the middle of the Si₃N₄ core. It consisted of CdSeS/ZnS QDs sandwiched by 20 nm-thick SiO₂ layers which are expected to contribute to thermal insulation of the QDs from the Si₃N₄ core. After growing the bottom half structure of the waveguide, the sample was unloaded and was covered by the QD colloid and left in the atmospheric environment until complete vaporization of hexane. Then, the sample was reloaded into the reactor and the top half of the waveguide was grown on it. The deposition temperature was set to 150 °C to avoid any damage to the organic coating of the QDs. The waveguide was etched through the whole layer structure down to the substrate. The height and width of the waveguide were $\sim 9 \mu\text{m}$, and the total waveguide length was 8 mm.

Fig. 11(c) clearly confirms the presence of the QDs in the middle of the core along the waveguide, with QDs fluorescence well-confined in the waveguide core. While spatial distribution of the QDs was not very uniform, QDs were securely located in the waveguide and exhibited strong emission from the middle of the core, as indicated with an arrow in the bottom panel of Fig. 11(c). However, because of the nonuniformity in QD distribution, the surface morphology was degraded.

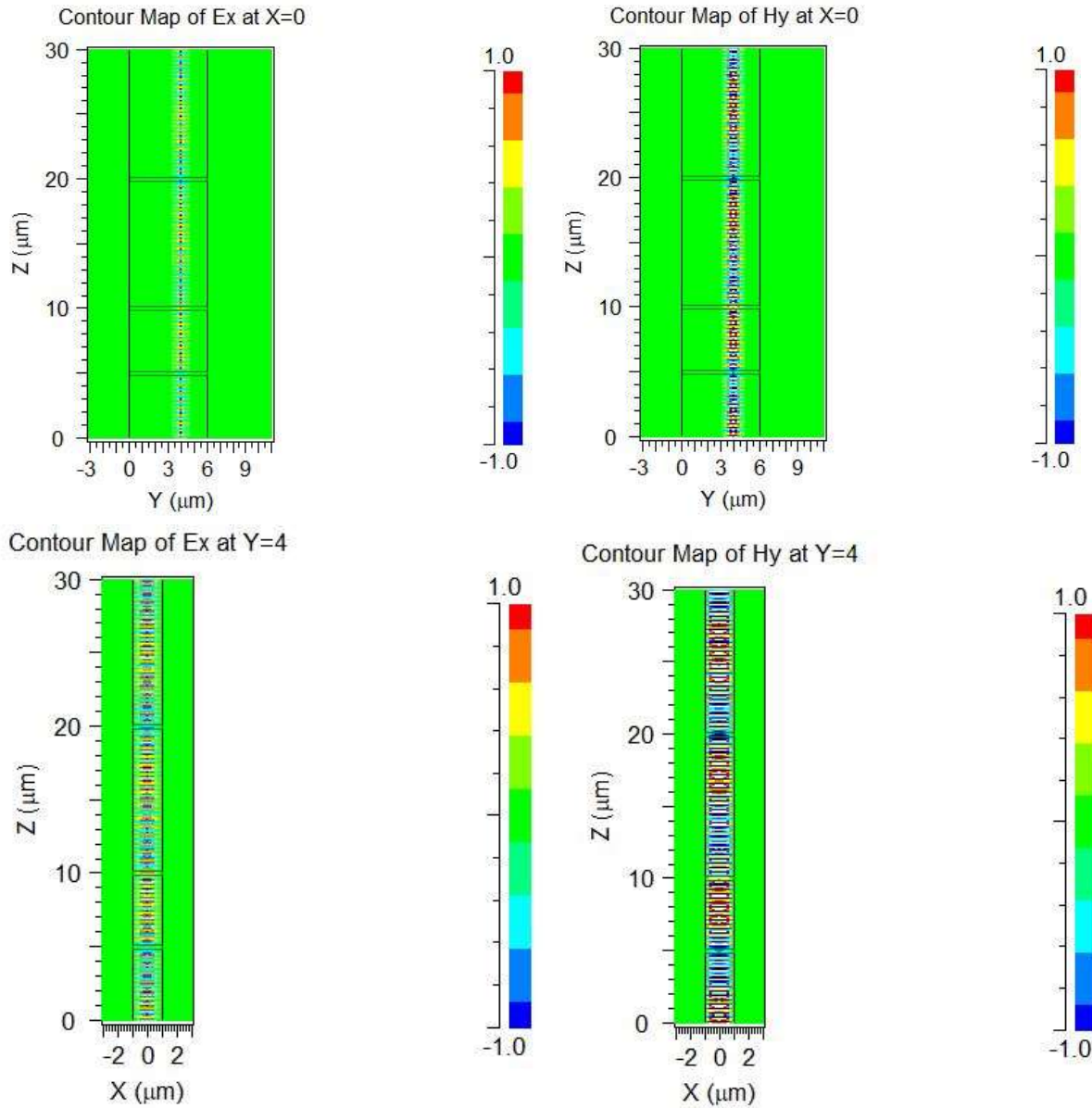


Fig. 10. 3D simulation results for the waveguide structure, showing the E_x (left) and H_y (right) component distributions for the fundamental TE-like mode of the waveguide at fixed y -positions of interest. The color code indicates the values of the E_x and H_y components.

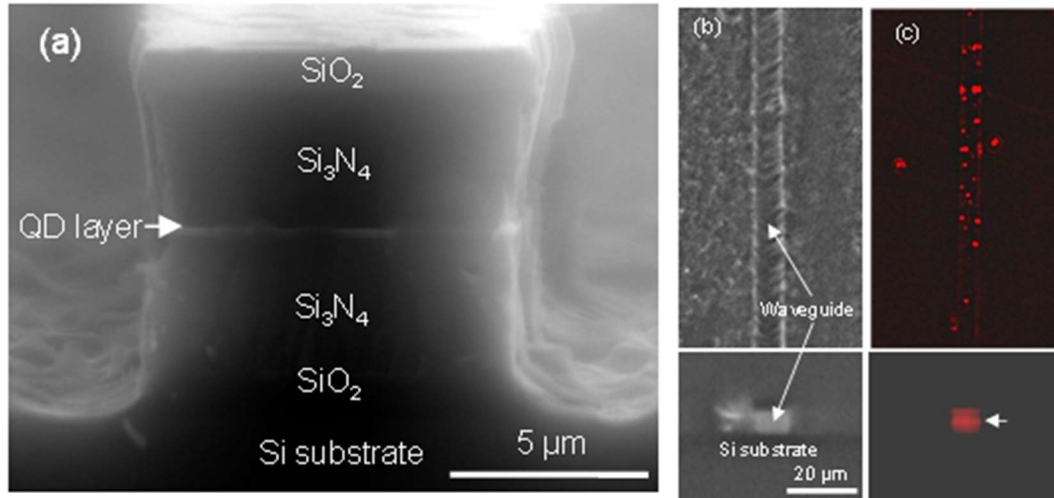


Fig. 11. (a) Cross-sectional SEM image of a waveguide with the QD layer in the middle of the Si₃N₄ core. (b) Optical, and (c) fluorescence microscope images of the same area of the waveguide. The fluorescence micrographs (c) were captured with 450 nm excitation. The top and bottom panels in (b) and (c) are top-down and cross-sectional views, respectively.

4. LASER COOLING EXPERIMENTS

4.1 Luminescence thermometry method

4.1.1 Measurement setup for luminescence thermometry

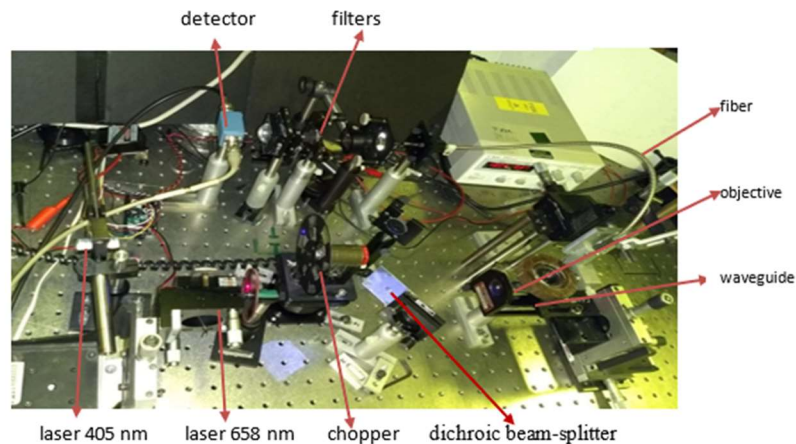


Fig. 12. Setup for laser cooling demonstration.

The set up for the measurements is shown in Fig. 12. Major components are two semiconductor lasers (one emitting at 658 nm for pumping and the other emitting at 405 nm for probing the waveguide), a photodetector, a chopper, and a lock-in amplifier. Probing and pumping laser beams are combined by dichroic beam-splitter and coupled into the waveguide by an objective. Probing and pumping lasers are modulated by the chopper such a way that they exhibit 180° phase shift (one is on when the other is off). Filters block pumping and probing light and allow Stokes and anti-Stokes PL emission collection from the excited QDs.

4.1.2 Luminescence thermometry concept

Fig. 13(a) is a schematic illustration of the measurement setup for the luminescence thermometry. Fig. 13(b) represents the expected signal plots vs. time of the pump laser, QD temperature, probe laser, reference of lock-in amplifier, and measured fluorescence vs. time during pumping/probing cycles.

When the cooling by anti-Stokes effects begins with the QDs in the middle of the core, induced by the pumping starting at the time t_1 [first row of Fig. 13(b)], the temperature of the sample drops down [second row of Fig. 13(b)]. At t_2 when the pump is off, the cooling process is terminated and the sample starts to warm due to heat transfer from the environment. At this moment, probing laser is on [third row of Fig. 13(b)] and the PL signal can be measured. The PL intensity decreases with increasing temperature as demonstrated in Fig. 8(a). Signals from the pump and probe lasers should not overlapping in time, due to Stokes and anti-Stokes PL interference.

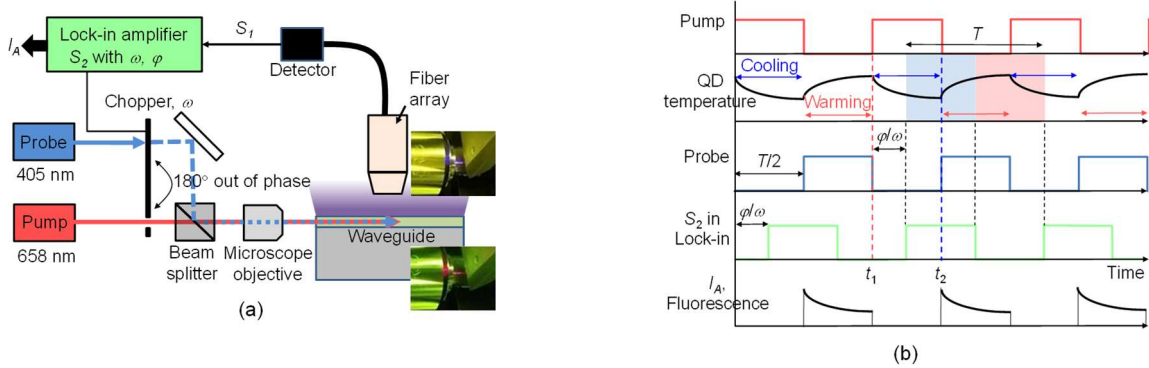


Fig. 13. A schematic illustration of the measurement setup for luminescence thermometry (a). A plot of signal for various components vs. time (b).

The slope of the fluorescence signal relates to the temperature change in the waveguide: negative slope corresponds to cooling by pump and then warming due to the environment [fourth row in Fig. 13(b)]. In case of laser warming effect the graph would be the opposite: positive slope would indicate warming by pump and then cooling due to the environment. Note, that QD temperature and corresponding fluorescence signal are shifted by a half period ($T/2$) relative to the probe signal, which means that pump and fluorescence signals should be $\sim 90^\circ$ shifted in phase. Lock-in amplifier was used to determine such a phase change of fluorescence signal relative to the original probe signal.

The signal collected by the detector, $S_1 = A_1 \sin(\omega t + \varphi)$, can be written as:

$$S_1 = P_{s,pump} + P_{s,probe} + S_w \quad (1)$$

where $P_{s,pump}$ and $P_{s,probe}$ are the measured scattered power from the pump and probe lasers in the setup, respectively, and S_w is the fluorescence in the waveguide. The $P_{s,pump}$ and $P_{s,probe}$ are greatly attenuated by band-pass filter to increase portion of S_w collected by the photodetector. The reference signal, S_2 , which the chopper generates for the lock-in amplifier with the angular frequency ω and the phase shift φ set equal to zero, can be written as $S_2 = A_2 \sin(\omega t)$.

Ultimately, the lock-in amplifier measures the autocorrelation A , expressed as

$$A = |A| \cdot \exp(i\varphi) \propto \int_t^{t+T} S_1 \cdot S_2 dt' \sim \int_t^{t+T} S_w \cdot S_2 dt' \quad (2)$$

In general, A is a complex number which is proportional to the amplitude of signal S_w and indicating its phase shift. The amplitude of S_w reflects decay rate of the fluorescence that includes the information on cooling and warming rates of the given nanoemitters, directly related to anti-Stokes effects for laser cooling. In the Fourier transform of the fluorescence intensity decreasing with time (corresponding to laser cooling when the pump laser is on and to sample warming when the pump laser is off), φ in Eq. (2) as measured by the lock-in amplifier must be negative, as illustrated in Fig. 13(b). In contrast, the fluorescence intensity increasing with time (corresponds to laser warming when the pump laser is on and to sample cooling when the pump laser is off) would induce a positive φ . To our knowledge, this idea of detecting laser cooling effect has not been explored yet and further theoretical analysis may be required to extract the anti-Stokes effects from the experimental data quantitatively.

4.2 Laser cooling results

The cooling and warming of the waveguide primarily depends on the pump laser power. If the power is excessively high, causing saturation of QDs, warming should occur instead of cooling. Cooling should dominate warming if the pump laser power is optimally controlled below the transition point to warming. Fig. 14(a) is a plot of φ vs. power of the pump laser P_p , measured at room temperature in the setup of Fig. 13(a). The maximum pump power P_p was 150 mW. As

expected from Fig. 13(b), the variation of φ with P_p provides the information about the cooling by anti-Stokes effects from the CdSeS/ZnS QDs embedded in the middle section of the Si₃N₄ core. The inset of Fig. 14(a) is a screen capture of the lock-in amplifier during phase measurement. Since the phase for the entire power range was consistently positive, the waveguide was in warming state when the pump laser was on.

Although the phase is increased with P_p , it behaves differently depending on P_p . At low ($< \sim 30$ mW) power, φ increases very rapidly with P_p . That is explained by the fact that $P_{s,pump}$ compensates $P_{s,probe}$ signal phase shift induced by warming from the probe laser. Further, the phase is constant with pump power for the mid-power range. This reduced slope implies the partial suppression of warming by the cooling that results from the anti-Stokes effects of the QD layer. The phase increases again for power above 70 mW, because eventually the QDs start to saturate reducing efficiency of cooling. Thus, the change of the slope in the mid-power range in Fig. 14(a) can be regarded as an indirect evidence for the laser cooling by the CdSeS/ZnS QDs embedded in the waveguide.

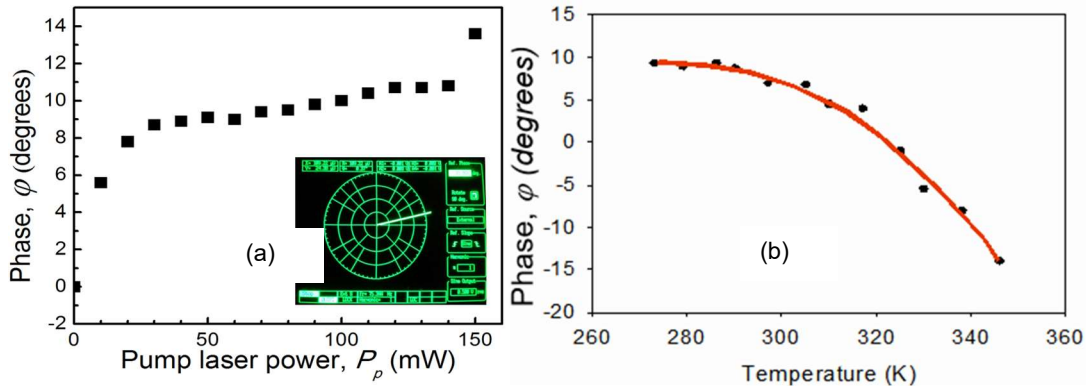


Fig. 14. (a) A plot of fluorescence phase shift vs. pump laser power at 300 K, measured by the lock-in amplifier in the setup. Inset: A screen capture of the lock-in amplifier that shows a positive φ with respect to the x -axis (the reference for φ is set by the exclusive coupling to the probe laser) under the coupling to the pump laser. (b) A plot of fluorescence phase shift vs. waveguide environment temperature, with the constant pump laser power of 30 mW.

We have found the evidence of optical cooling at elevated temperatures of the waveguide, which is consistent with the strong temperature dependence of ASPL, as shown in Fig. 8(b). The change of phase φ with increasing temperature of the waveguide environment from 270 K to 350 K was registered. This dependence is shown in Fig. 14(b). A change in sign of the phase φ was observed at the temperatures above 320 K, which is a direct evidence of local optical cooling. The physical mechanism can be explained in the following way. As can be seen in Fig. 8(b), the PL peak occurs at 630 nm. The pump laser available for the experiments emitted at 658 nm. This corresponds to 0.078 eV anti-Stokes shift. Since the thermal energy kT at room temperature of 25.7 meV was much smaller than the anti-Stokes shift of 78 meV, the efficiency of phonon-exciton coupling was very low and insufficient for laser cooling. That problem was solved by heating the waveguide environment to the temperature above 320 K, matching kT with the anti-Stokes shift. This allowed phonon-exciton coupling to be enhanced and laser cooling to be observed.

The strong temperature dependence of ASPL shown in Fig. 8(b) is consistent with the predicted enhancement of anti-Stokes emission with increasing temperature [11]. Near-unity quantum efficiency of QDs is the necessary condition for laser cooling [11]. Room-temperature quantum efficiency of CdSeS/ZnS QDs exceeding 50% for UV excitation was reported by the manufacturer. We point out that ~ 1.5 to ~ 2 times increase in quantum efficiency has recently been reported in CdSe/CdS QDs with the excitation wavelength changing from UV to visible [12], [13]. These observations combined with the strong temperature enhancement of ASPL [Fig. 8(b)], make near-unity quantum efficiency of CdSeS/ZnS QDs excited at 658 nm at the waveguide temperatures higher than 320 K a reasonable goal.

5. CONCLUSIONS

In conclusion, the laser cooling effects in a SiO₂/Si₃N₄/SiO₂ waveguide structure with embedded CdSeS/ZnS QDs as nanoemitters have been investigated. CdSeS/ZnS QDs have been successfully embedded into the core of the waveguides by thin film deposition and confirmed as promising nanoemitters for laser cooling due to the strong anti-Stokes effects. A direct evidence of local optical cooling in the waveguide structure has been demonstrated with a luminescence thermometry based on the detection of photoluminescence signal phase change versus power of the pumping laser using a lock-in amplifier.

6. ACKNOWLEDGEMENTS

This work was supported by the Office of Naval Research Grants N00014-17-1-2975 and N00014-19-1-2117, and by the Navy HBCU/MI Program Grant N00014-18-1-2739. This work was performed, in part, at the Center for Integrated Nanotechnologies, an Office of Science User Facility operated for the U.S. Department of Energy (DOE) Office of Science by Los Alamos National Laboratory (Contract DE-AC52-06NA25396) and Sandia National Laboratories (Contract DE-NA-0003525), under the Projects #2017AU0108 “*Characterization of Bactericidal Nanoparticles for Gingivitis Prevention and Treatment*” and #2018BU0135 “*Studies of Cytotoxicity and Bactericidal Effects of Colloidal Nanoparticles on Hybrid Oral Biofilms*”. The views expressed in this paper do not necessarily represent the views of the U.S. DOE or the United States Government. The authors would like to express their gratitude to the Optiwave Systems, Inc. for the generous terms of the Academic License Agreement allowing for a free use of OptiSuite.

REFERENCES

- [1] X. L. Ruan and M. Kaviani, “Advances in laser cooling of solids”, *Journal of Heat Transfer* **129** (#1), pp. 3-10, Jan. 2007.
- [2] G. Nemova and R. Kashyap, “Laser cooling of solids”, *Reports on Progress in Physics* **73** (#8), Art. 086501, 2010.
- [3] D. V. Seletskiy, R. Epstein, and M. Sheik-Bahae, “Laser cooling in solids: Advances and prospects”, *Reports on Progress in Physics* **79** (#9), Art. 096401, 3 Aug. 2016.
- [4] R. I. Epstein, M. I. Buchwald, B. C. Edwards, T. R. Gosnell, and C. E. Mungan, “Observation of laser-induced fluorescent cooling of a solid”, *Nature* **377** (#6549), pp. 500-503, 12 Oct. 1995.
- [5] X. S. Zhu and N. Peyghambarian, “High-power ZBLAN glass fiber lasers: Review and prospect”, *Advances in OptoElectronics* **2010**, Art. 501956, 2010 (23 pp.).
- [6] S. Adachi, “Lattice thermal conductivity of group-IV and III-V semiconductor alloys”, *Journal of Applied Physics* **102** (#6), Art. 063502, 15 Sep. 2007.
- [7] D. H. Li, J. Zhang, X. J. Wang, B. L. Huang, and Q. H. Xiong, “Solid-state semiconductor optical cryocooler based on CdS nanobelts”, *Nano Letters* **14** (#8), pp. 4724-4728, Aug. 2014.
- [8] J. Zhang, D. H. Li, R. J. Chen, and Q. H. Xiong, “Laser cooling of a semiconductor by 40 kelvin”, *Nature* **493** (#7433), pp. 504-508, 24 Jan. 2013.
- [9] Q. Zhang, X. F. Liu, M. I. B. Utama, G. C. Xing, T. C. Sum, and Q. H. Xiong, “Phonon-assisted anti-Stokes lasing in ZnTe nanoribbons”, *Advanced Materials* **28** (#2), pp. 276-283, 13 Jan. 2016.
- [10] R. S. Fontenot, V. K. Mathur, J. H. Barkyoumb, C. E. Mungan, and T. N. Tran, “Measuring the anti-Stokes luminescence of CdSe/ZnS quantum dots for laser cooling applications”, in *Tri-Technology Device Refrigeration (TTDR)* (R. I. Epstein, B. F. Andresen, M. P. Hehlen, I. N. Rühlich, M. Sheik-Bahae, and T. Fraser, Eds.), Baltimore, MD, 17-21 Apr. 2016, *Proceedings of SPIE* **9821**, Art. 982103.
- [11] Y. P. Rakovich, J. F. Donegan, M. I. Vasilevskiy, and A. L. Rogach, “Anti-Stokes cooling in semiconductor nanocrystal quantum dots: A feasibility study”, *Physica Status Solidi A* **206** (#11), pp. 2497-2509, Nov. 2009.
- [12] D. Geissler, C. Würth, C. Wolter, H. Weller, and U. Resch-Genger, “Excitation wavelength dependence of the photoluminescence quantum yield and decay behavior of CdSe/CdS quantum dot/quantum rods with different aspect ratios”, *Physical Chemistry Chemical Physics* **19** (#19), pp. 12509-12516, May 2017.
- [13] I. V. Martynenko, A. S. Baimuratov, V. A. Osipova, V. A. Kuznetsova, F. Purcell-Milton, I. D. Rukhlenko, A. V. Fedorov, Y. K. Gun'ko, U. Resch-Genger, and A. V. Baranov, “Excitation energy dependence of the photoluminescence quantum yield of core/shell CdSe/CdS quantum dots and correlation with circular dichroism”, *Chemistry of Materials* **30** (#2), pp. 465-471, Jan. 2018.